Nanoelectronics and Its New Materials – A NEW ERA OF NANOSCIENCE

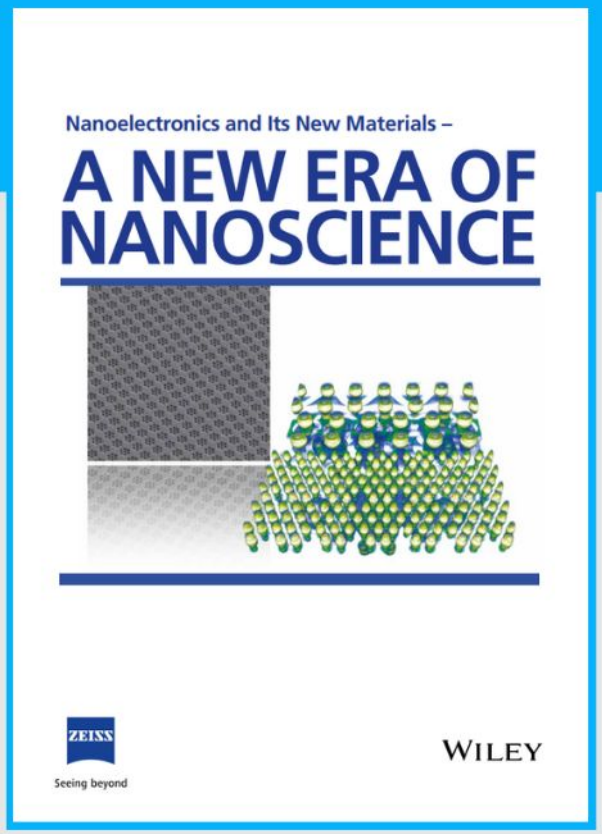

Discover the recent advances in electronics research and fundamental nanoscience.

Nanotechnology has become the driving force behind breakthroughs in engineering, materials science, physics, chemistry, and biological sciences. In this compendium, we delve into a wide range of novel applications that highlight recent advances in electronics research and fundamental nanoscience. From surface analysis and defect detection to tailored optical functionality and transparent nanowire electrodes, this eBook covers key topics that will revolutionize the future of electronics.

To get your hands on this valuable resource and unleash the power of nanotechnology, simply download the eBook now. Stay ahead of the curve and embrace the future of electronics with nanoscience as your guide.

ZEISS

Seeing beyond

WILEY

NANO · MICRO small
www.small-journal.com

Cooperative Synthesis of Raspberry-Like Covalent Organic Framework-Polymer Particles with a Radial Single-Crystal Grain Orientation

*Pauline Salaün, Alexandre Fadel, Mario Pelaez-Fernandez, Bahae-Eddine Mouloud, Jean-François Tahon, Christophe Volkringer, Ahmed Addad, Patrice Woisel, and Gaëlle Le Fer**

Despite many efforts devoted toward the design of covalent organic frameworks (COFs) at the framework level by selecting the building blocks, their organization in the nano to meso regimes is often neglected. Moreover, the importance of processability for their applications has recently emerged and the synthesis of COF nanostructures without agglomeration is still a challenge. Herein, the first example of hybrid COF-polymer particles for which polymers are used to manipulate the 2D COF growth along a specific direction is reported. The study examines how the nature, chain-end functionality, and molar mass of the polymer influence the shaping of hybrid 2D boronate ester-linked COF-polymer particles. Catechol-poly(*N*-butyl acrylate) leads to the self-assembly of crystallites into quasi-spherical structures while catechol-poly(*N*-isopropylacrylamide) mediates the synthesis of raspberry-like COF-polymer particles with radial grain orientation. Scanning and transmission electron microscopies (SEM and TEM) and 4D-STEM-ACOM (automated crystal orientation mapping) highlight the single-crystal character of these domains with one plane family throughout the particles. Interestingly, the presence of PNIPAm on the particle surface allows their drying without co-crystallization and enables their resuspension. Kinetic investigations show that catechol-P*n*BuA acts as a modulator and catechol-PNIPAm induces a template effect, introducing supramolecular self-assembly properties into particles to create new morphologies with higher structural complexity, beyond the framework level.

1. Introduction

Reticular synthesis defines how molecular units are linked in 2D or 3D to build crystalline framework structures. Such reticulation of symmetric organic molecules through directional covalent bonds has led to the development of covalent organic frameworks (COFs), anemerging class of crystalline light materials with programmable and permanent porosity.[1] The geometry of the monomers and the orientation of their reactive groups determine network's dimensions and topology, and defines the pore size.[2] The intrinsic characteristics of COFs, i.e., their pore size and shape, their porosity, their high specific surface area, and their lightness make them materials that first found applications related to gas storage[3] and molecular separation.[4–6] The incorporation of functional units in their structure has tailored COF chemistry for numerous potential applications (catalysis,[7] molecular recognition and detection,[8,9] energy storage,[10] optoelectronic devices,[11] encapsulation and delivery of bioactive molecules[12,13]).

P. Salaün, M. Pelaez-Fernandez, B.-E. Mouloud, J.-F. Tahon, A. Addad, P. Woisel, G. Le Fer
UMR 8207 – UMET – Unité Matériaux Et Transformations, CNRS, INRAE
University of Lille
Ecole Centrale, Lille F-59000, France
E-mail: gaelle.lefer@univ-lille.fr

A. Fadel
FR 2638 – IMEC – Institut Michel-Eugène Chevreul
CNRS
INRAE
Université d'Artois, University of Lille
F-59000, Ecole Centrale Lille, France

C. Volkringer
UMR 8181 – UCCS – Unité de Catalyse et Chimie du Solide
CNRS
Univ. Artois
University of Lille
Centrale Lille, Lille F-59000, France

The ORCID identification number(s) for the author(s) of this article can be found under https://doi.org/10.1002/smll.202303697

DOI: 10.1002/smll.202303697

However, COFs suffer from significant limitations: they are by nature crosslinked materials and most of them are isolated at the macroscopic scale as insoluble powders. Such polycrystalline precipitates often do not fulfill the particular processing requirements, well-defined volumetric properties, and anisotropic alignment to be useful as materials for specific applications.[14] In addition, the COF nanostructures and their single or polycrystallinity character greatly influence their properties.[15] Despite many efforts devoted towards the design at the framework level by selecting the initial building blocks[16] and the dynamic covalent chemistry used,[17] the organization of COFs in the nano to meso regimes is often neglected.[18] Meso-materials (reticular structures at a length scale of 100 nm to 1000 nm) fill the gap between nano and bulk materials and combine the characteristics common to both.[19] Meso-objects can also be obtained from the self-assembly of sub-units, leading to the enhancement of properties or the birth of new ones that cannot be provided by the crystal alone.[19] Consequently, synthetic approaches allowing the control of nucleation and growth of COF crystallites and their self-assembly into particles, have received attention from researchers. In this context, Dichtel and co-workers[20] found that the addition of nitrile cosolvent avoids precipitation of 2D boronate ester-linked COFs and stabilizes them into colloidal suspension. Efforts have been made to synthesize large framework single crystals[21,22] but their unfavorable mechanical properties prevent their direct use.[19] Nevertheless, only a handful of studies report the design of uniform well-defined spheres with a higher level of complexity, such as compartmentalization, to organize the matter up to the mesoscale. For example, solution-processable uniform spherical imine-linked[23,24] and β-ketoenamine linked COF particles[24] were synthesized with controlled size up to 700 nm. Hybrid core-shell structures combining metal oxide and COF on the surface, with control of the shell thickness and photothermal conversion ability were also obtained.[25] In addition, stable hollow-spherical COFs from nano to micrometric size were obtained via an Ostwald ripening mechanism and without sacrificial template.[26–28] Moreover, Lu and co-workers[29] reported the synthesis of spherical microparticles of imine COFs with a radial orientation of crystals. They hypothesized a self-assembly mechanism of rod-like crystallites. Controllable synthesis of COF particles with complex and uniform morphology is paramount but still challenging, the development of straightforward synthetic strategies allowing the organization of the COF crystallites on the nano and mesoscale is highly desirable.

We report an original approach combining COF and linear polymers. Surprisingly, while the development of COF-polymer composites gained increasing attention in the last few years, the nature of the polymer used is still limited to poly(ethylene glycol) or poly(vinylpyrrolidone).[30] Moreover, the attention was paid on linear polymer-embedded COFs, in which polymers are confined into the pore channels of COFs (by physical diffusion/mixing,[31] grafting[32] or by in situ polymerization[33–35]), and on the synthesis of polyCOFs through condensation reaction using both small molecules and linear polymer derivatives as building blocks.[36]

Herein, we present the solvothermal synthesis of colloidal 2D boronate ester-linked COF-5 in the presence of polymers. The addition of a monofunctionalized modulator was previously reported as a way to control nucleation-growth and COF "external" functionalization,[37,38] we hypothesized that chain-end functionalized macromolecular chains could covalently attach to COF particles and influence their size and shape. The stable suspensions of COF-polymer particles were fully characterized by dynamic light scattering (DLS), wide-angle X-ray scattering (WAXS), scanning and transmission electron microscopies (SEM and TEM), and 4D STEM-ACOM (automated crystal orientation mapping). While alkyne-poly(*N*-butyl acrylate) (alkyne-P*n*BuA) prevented the COF formation, catechol-poly(*N*-butyl acrylate) (catechol-P*n*BuA) led to the self-assembly of crystallites into quasi-spherical structures and catechol-poly(*N*-isopropylacrylamide) (PNIPAm) mediated the synthesis of raspberry-like COF-polymer particles with a radial single-crystal grain orientation. Such hybrid COF-PNIPAm particles can be stored as dried powder and resuspended in acetonitrile with no aggregation. This approach represents the first example of hybrid COF-polymer particles for which polymers are used to manipulate the 2D COF growth along a specific crystalline direction.

2. Results and Discussion

Recently, the synthesis of colloidal boronate ester-linked COF-5 suspensions was performed but the particles obtained are limited in size or required the continuous addition of reagents over weeks. Moreover, the resulting particles were not isolable, and the removal of the organic solvent mixture led to an insoluble polycrystalline film.[20,21] Inspired by the few publications reporting the polymer-assisted synthesis of metal–organic frameworks (MOFs) using polymers as templates to provide access to a wider variety of MOF morphologies and sizes,[39–42] we combined COF-5 and chain-end functionalized polymers to obtain large spherical particle with complexes morphologies. First, we synthesized colloidal COF-5, the obtained particles were imaged by SEM and TEM (Figure S1, Supporting Information). Aggregates of anisotropic and polycrystalline particles randomly deposited and with no specific fringe orientation were observed. Then, various polymers were synthesized to examine how the nature, chain-end functionality, and molar mass of the macromolecular grafts influence the shaping of 2D boronate ester-linked COF-polymer particles. A catechol chain-end functionality was first chosen for its ability to act as a modulating agent in the COF-5 synthesis.[38] Monofunctional catechol-poly(*N*-butyl acrylate) (catechol-P*n*BuA) was synthesized by Reversible Addition-Fragmentation chain-Transfer (RAFT) polymerization (Table S1, Supporting Information). A degree of polymerization ($\overline{DP_n}$) $\approx$ 30 and a molar mass of 4400 g•mol^{-1} were obtained as assessed by ^{1}H NMR (Figure S2, Supporting Information). Analysis by size exclusion chromatography (SEC) in THF revealed an apparent molar mass of 3600 g mol^{-1} in agreement with the NMR value and a narrow dispersity ($Đ$) of 1.17 that confirmed the well-controlled behavior of the polymerization process (Figure S3, Supporting Information). Then, monomer solutions of 1,4-phenylenebis(boronic acid) (PBBA, 2.25 mM) and 2,3,6,7,10,11-hexahydroxytriphenylene (HHTP, 1.5 mM) in CH_3CN:1,4-dioxane:mesitylene (80/16/4, v/v/v) were prepared, and variable amounts of catechol-P*n*BuA (equiv = [catechol-P*n*BuA]/[PBBA]) were added to these solutions. The COF-catechol-P*n*BuA syntheses were performed at 70 °C for 24 h

under atmospheric pressure. Visually stable milky suspensions were obtained. After the removal of the polymer excess, wide-angle X-ray scattering (WAXS) experiments were used to identify the conditions for which the crystallinity of the colloids is maintained in the presence of catechol-P*n*BuA. **Figure 1**A and Figure S4 (Supporting Information) show Bragg diffraction peaks at $q = 0.24$ and 0.42 Å^{-1}, corresponding to the (100) and (110) diffraction planes of a hexagonal lattice with in-plane lattice parameters $a = b = 29.9$ Å.

These values correspond with those measured (29.7 Å) and calculated (30.0 Å) previously reported for COF-5 powders and colloids.[1,21] Interestingly, the addition of 0.045 equiv. of catechol-P*n*BuA/PBBA led to more intense (100) and (110) peaks compare to colloidal COF-5 without polymer (Figure 1A) indicating that the crystallinity of these COF-catechol-P*n*BuA is higher compared to COF-5. On the contrary, the mixtures containing 0.090 and 0.14 equiv. of catechol-P*n*BuA/PBBA led to less crystallized suspensions suggesting a higher polymer ratio disturbed the COF formation (Figure S4, Supporting Information). For 0.045 equiv., the formation of COF-catechol-P*n*BuA particles with an average hydrodynamic radius (R_h) of 60 nm, similar to COF-5 obtained without polymer, was confirmed by dynamic light scattering (DLS) (Figure 1B). Scanning and transmission electron microscopies (SEM and TEM) were used to visualize their size, shape, and crystallinity. SEM micrographs (Figure 1C and Figure S5, Supporting Information) show particles of about 70 nm in radius with a quasi-spherical structure. TEM imaging in bright field (BF) mode (Figure 1D) reveals that each particle is made of assembled individual anisotropic sub-units. Moreover, micrographs obtained in high-angle annular dark-field scanning transmission electron microscopy (HAADF-STEM) mode (Figure 1E,F) clearly show that sub-units are single-crystalline since continuous lattice fringes are observed. As measured by fast Fourier transform (FFT; inserts in Figure 1E,F), the fringe spacing is about 23 Å, fitting d_{100} for COF-5. To highlight the role of the catechol chain-end moiety in the COF-5 synthesis mechanism, an alkyne-P*n*BuA polymer with a $\overline{DP_n}$ 27 as assessed by ^{1}H NMR (Figure S7, Supporting Information) and a $Đ$ of 1.19 (Figure S3, Supporting Information) was prepared using alkyne-CTA as RAFT agent (Figure S6, Supporting Information) and then added for the colloidal COF-5 synthesis. Visually stable milky suspensions were also obtained. The WAXS trace (Figure 1A) does not show Bragg diffraction peak, indicating a lack of crystallinity even if particles with a R_h of 60 nm were also obtained (Figure 1B). Consequently, the presence of P*n*BuA polymer without the catechol functionality prevented the crystallization, the catechol moiety acted as a modulating agent, as previously reported for monofunctional small organic molecules,[37] and enhanced the COF material quality. In addition, the high quality of COF-5 and COF-catechol-P*n*BuA materials was confirmed by N_2 physisorption with respective BET surface areas of 1423 m^2 g^{-1} and 158 m^2 g^{-1} (Figure S8, Supporting Information).

Then, to examine how the nature of the polymer used can influence the COF-polymer formation, we move to catechol-PNIPAm polymer. PNIPAm was chosen for its good solubility in the CH_3CN/dioxane/mesitylene mixture and for the presence of amide functions able to form hydrogen bonds with alcohol groups from the monomers.[43,44] Monofunctional catechol-PNIPAm polymers with $\overline{DP_n}$ 25, 50, and 100, respectively named catechol-PNIPAm$_{25}$, catechol-PNIPAm$_{50}$, and catechol-PNIPAm$_{100}$ were synthesized by RAFT polymerization and fully characterized by ^{1}H NMR (Figures S9–S11, Supporting Information) and SEC (Figure S12, Supporting Information). First, variable amounts of catechol-PNIPAm$_{25}$ (equiv = [catechol-PNIPAm]/[PBBA]) were added to HHTP and PBBA solutions, triggering an instantaneous cloud that indicates polymer/monomer interactions. Visually stable milky suspensions were obtained after reaction at 70 °C for 24 h under atmospheric pressure. After the removal of the polymer excess, WAXS experiments were performed. As previously observed for COF-catechol-P*n*BuA, the addition of 0.045 equiv. of catechol-PNIPAm$_{25}$/PBBA led to more intense (100) and (110) Bragg peaks compare to colloidal COF-5 without polymer (Figure 1A) indicating a higher crystallinity for these COF-catechol-PNIPAm$_{25}$ (Figure S13, Supporting Information). 0.045 equiv. of catechol-PNIPAm/PBBA was also added for $\overline{DP_n}$ 50 and 100, **Figure 2**A shows Bragg diffraction peaks at $q = 0.24$ Å^{-1} and 0.42 Å^{-1} broadening and decreasing in intensity as the $\overline{DP_n}$ increased, indicating lower crystallinity. COF-catechol-PNIPAm particles were characterized by DLS, monomodal size distributions with R_h of 300 nm, 250 nm and 200 nm were obtained for PNIPAm $\overline{DP_n}$ 25, 50, and 100, respectively (Figure 2B).

These COF-catechol-PNIPAm particles were imaged by SEM (**Figure 3** and Figures S14–S16, Supporting Information). The micrographs reveal the formation of raspberry-like particles made of spherical and monodispersed nano-sized sub-units more defined as the PNIPAm $\overline{DP_n}$ increases.

High-resolution TEM imaging was used to investigate the nanostructure and crystallinity of the COF-catechol-PNIPAm$_{25}$ particles (**Figure 4** and Figure S17, Supporting Information). Even at low magnification, discrete spherical particles were observed with visible lattice fringes (Figure 4A). Higher magnification (Figure 4B) reveals spherical sub-units forming an individual particle, each sub-unit being a single crystal with continuous fringes. Lattice-resolution micrograph (Figure 4C) clearly shows a specific radial fringe orientation from the center of the particles to the periphery with a lattice fringe spacing of about 24 Å (fitting d_{100} for COF-5). This distance was confirmed by the FFT (Figure 4D) of the micrograph in Figure 4A, the halo being due to the radial orientation of the single-crystals. Moreover, these particles show the expected hexagonal lattice fringes in the center, confirming the radial orientation through the entire thickness of the particles (Figure 4B,C). In addition, while the particles are randomly deposited on the grid they all present the same fringe spacing of 24 Å so they have the same orientation. To reinforce these observations about the crystal grain orientation, automated crystal orientation mapping (ACOM) by STEM was used.[45] A selected area (Figure 4E, left) was scanned and the diffraction pattern was recorded for every position. For example, Figure 4E, center shows three diffraction images from three color-coded regions of interest (red, green, blue). Due to their thickness, no diffraction image could be acquired in the particle centers. The combination of all the diffractions obtained allowed to produce the ACOM image (Figure 4E, right) with flowlines showing the continuity of the crystal structure and confirming the radial orientation of the single-crystal sub-units constituted the COF-catechol-

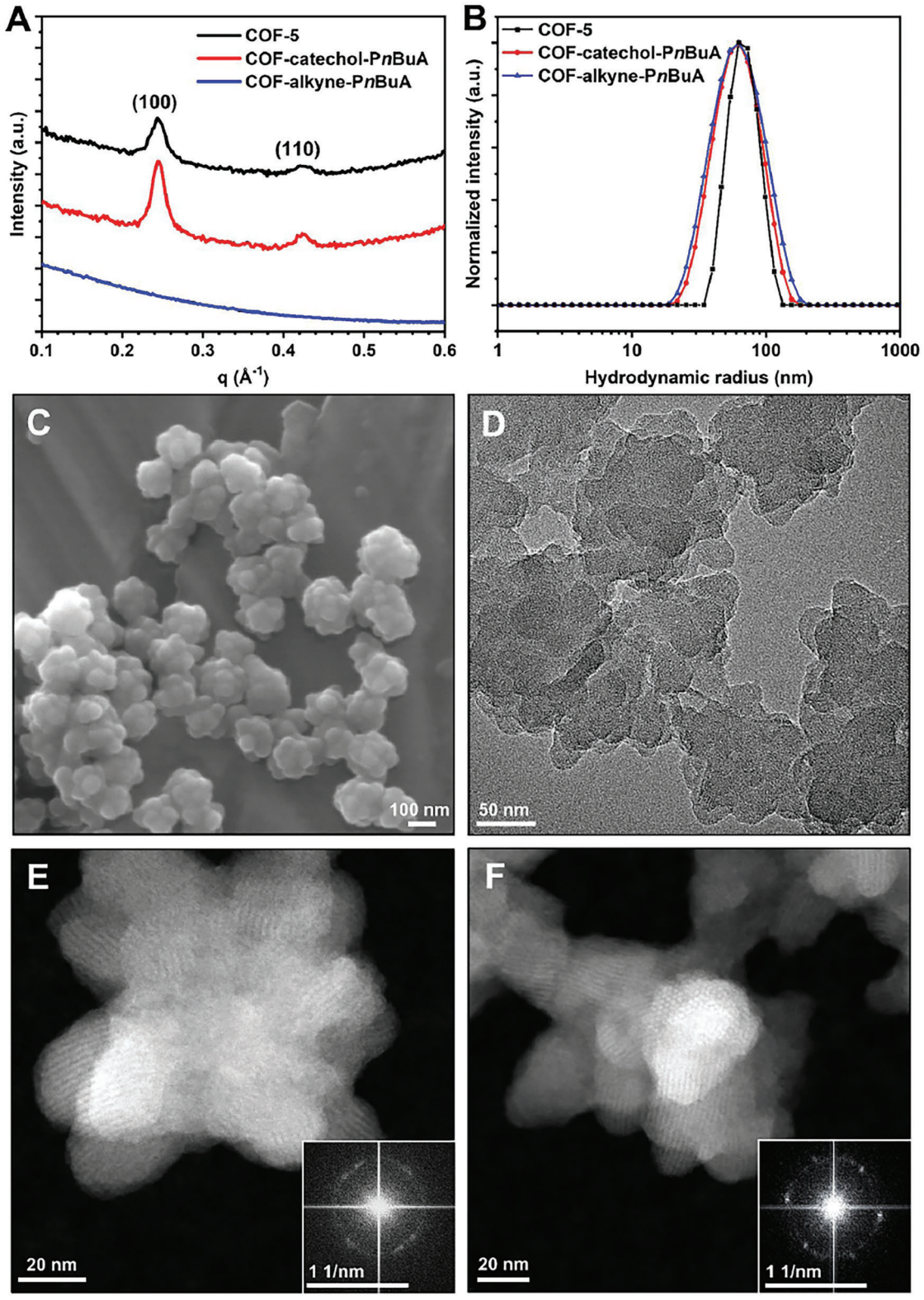

Figure 1. A) Wide-angle X-ray scattering traces for colloidal suspensions of COF-5 without polymer, COF-catechol-P*n*BuA, and COF-alkyne-P*n*BuA obtained with 0.045 equiv. of polymer/PBBA, B) hydrodynamic radius distribution by DLS of COF-5 particles without polymer, COF-catechol-P*n*BuA, and COF-alkyne-P*n*BuA obtained with 0.045 equiv. of polymer/PBBA, C) SEM micrograph of COF-catechol-P*n*BuA particles, D) BF-TEM micrograph of COF-catechol-P*n*BuA particles, E,F) lattice-resolution HAADF-STEM micrographs of COF-catechol-P*n*BuA particles with consistent lattice fringes extending across building sub-units. Insets: corresponding FFT images (fringe spacing ≈23 Å, d_{100}).

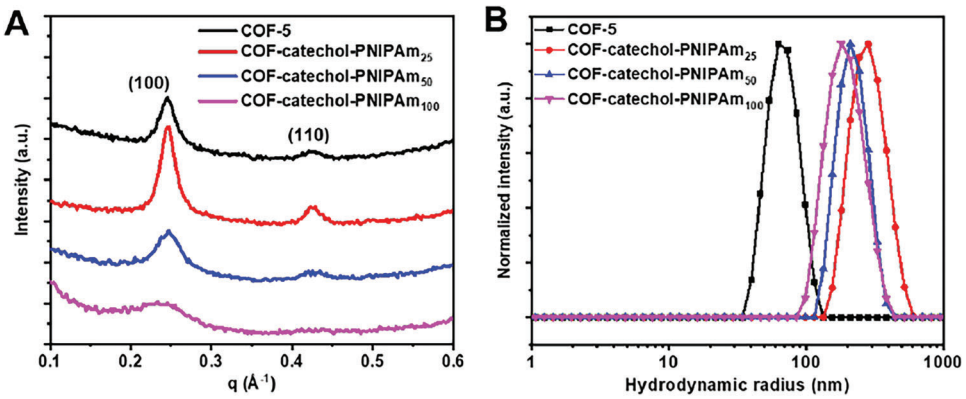

Figure 2. A) Wide-angle X-ray scattering traces for colloidal suspensions of COF-5 without polymer and COF-catechol-PNIPAm ($\overline{DP_n}$ = 25, 50, 100) obtained with 0.045 equiv. of polymer/PBBA, B) hydrodynamic radius distribution by DLS of COF-5 particles without polymer and COF-catechol-PNIPAm ($\overline{DP_n}$ = 25, 50, 100) obtained with 0.045 equiv. of polymer/PBBA.

$PNIPAm_{25}$ particles with one plane family throughout the particles. Moreover, the reconstituted averaged image of the diffraction patterns obtained (Figure 4E, right, inset) shows a halo, further supporting the progressive well-defined radial orientation. The unique distance obtained from the radial integration is 23.8 Å (Figure S18, Supporting Information) and matches the value obtained from both FFT and observation (about 24 Å, fitting d_{100} for COF-5). Same observations were made for COF-catechol-$PNIPAm_{50}$ particles that show also a radial fringe orientation with a lattice fringe spacing of 24 $Å^{-1}$ (fitting d_{100} for COF-5) and hexagonal lattices in the center of the particles (Figure S19, Supporting Information). This characteristic was confirmed by ACOM imaging (Figure S20, Supporting Information). However, for COF-catechol-$PNIPAm_{100}$ particles, due to their lower crystallinity as shown by WAXS experiment, no fringes are observed (Figure S21, Supporting Information). Nevertheless, all of the COF-catechol-PNIPAm samples exhibit accessible porosity (Figure S22, Supporting Information). COF-catechol-$PNIPAm_{25}$ material shows a BET surface area of 915 $m^2\ g^{-1}$ determined by N_2 physisorption at 77 K. Nonlocal density functional theory (NLDFT) analysis indicated a pore size of 26 Å, consistent with COF-5 powders. For COF-catechol-$PNIPAm_{50}$ and COF-catechol-$PNIPAm_{100}$, the low specific surface areas measured by N_2 at 77 K, respectively 2.5 and 10 $m^2\ g^{-1}$, are assigned to ultramicroporosity coming from the polymer chains blocking the pore and limiting the diffusion of N_2 (kinetic diameter of 3.8 Å). In that cases, CO_2 (kinetic diameter of 3.3 Å) at 298 K is a better probe to access to the porosity and to evaluate the accessible specific surface[46,47] and we measured BET surfaces of 25.8 and 6.8 $m^2\ g^{-1}$ for these composites. Interestingly, these results demonstrated a possible application in gas selectivity depending on the polymer used and its molar mass.

To determine the amount of catechol-P*n*BuA or catechol-PNIPAm polymers attached on the COF, we isolated the particles, degraded them until complete solubilization in deuterated solvent in presence of pinacol, and the resulting solutions were characterized by ^{1}H NMR spectroscopy. Contrary to COF-catechol-P*n*BuA for which no polymer was detected by ^{1}H NMR (Figure S23, Supporting Information; as previously reported for small organic modulator[48]), for COF-catechol-PNIPAm, the relative amounts of HHTP and catechol-PNIPAm could be estimated (Figures S24 and S25, Supporting Information). The catechol-PNIPAm:HHTP molar ratios are the following: 1:26, 1:22 and 1:33 for $\overline{DP_n}$ 25, 50, and 100 respectively (Table S2, Supporting Information), indicating lower polymer content for the higher $\overline{DP_n}$ likely due to the lower chain end accessibility allowing covalent grafting. The low incorporation of catechol-PNIPAm is clearly sufficient to modify the final shape and size of the particles obtained. We hypothesize that the small quantities of catechol-PNIPAm polymer in particles correspond to

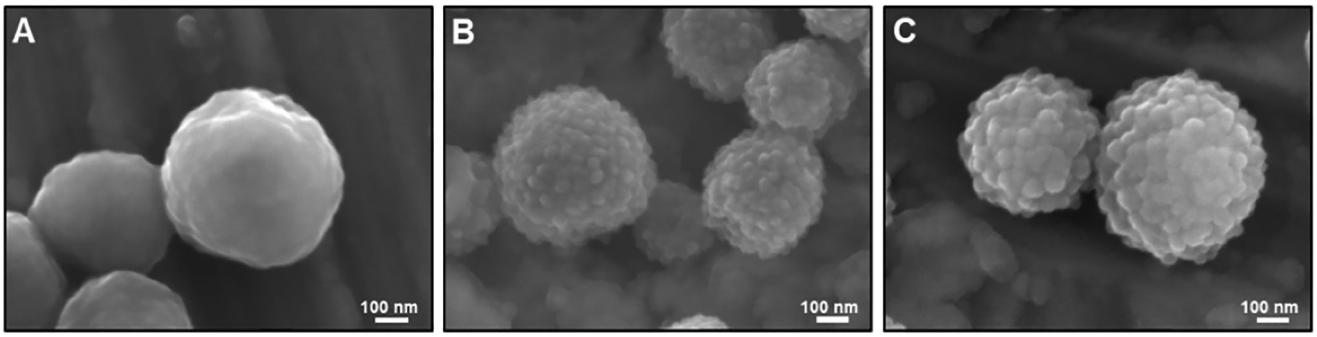

Figure 3. SEM micrographs of A) COF-catechol-$PNIPAm_{25}$ particles, B) COF-catechol-$PNIPAm_{50}$ particles, C) COF-catechol-$PNIPAm_{100}$ particles.

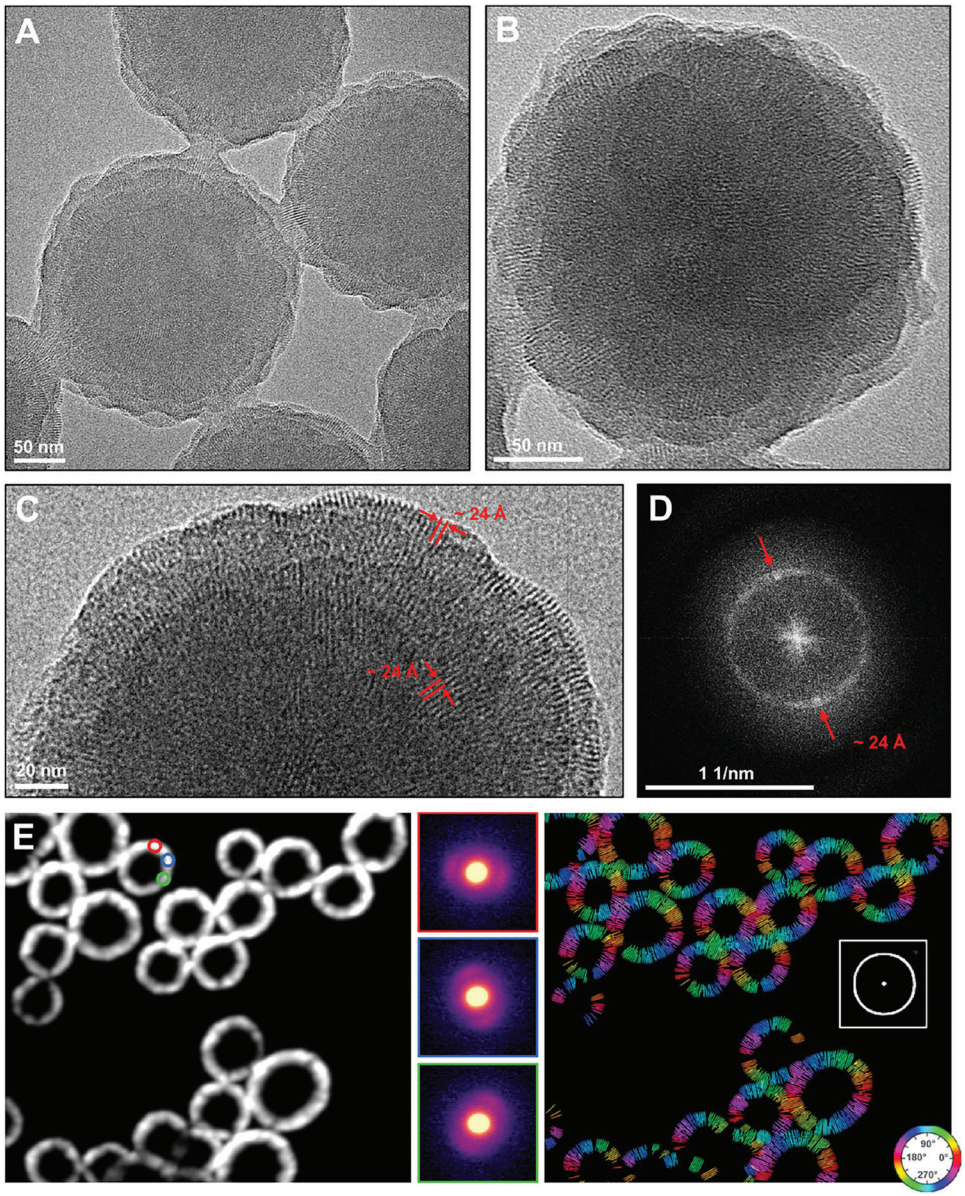

Figure 4. A) Low-magnification HRTEM micrograph of COF-catechol-PNIPAm$_{25}$ particles, B,C) lattice-resolution HRTEM micrographs of COF-catechol-PNIPAm$_{25}$ particles showing a specific radial fringe orientation from the center of the particles to the periphery with a lattice fringe spacing of about 24 Å (fitting d_{100} for COF-5). D) FFT image of micrograph A (fringe spacing ≈24 Å, d_{100}), E) virtual dark-field STEM micrograph of COF-catechol-PNIPAm$_{25}$ particles (left), diffraction images of the three color-coded regions of interest (fringe spacing ≈24 Å, d_{100}) (center) and corresponding ACOM image with flowlines confirming the radial fringe orientation (insert: averaged image of the diffraction patterns) (right).

macromolecular chains linked to dangling boronic esters at the edges of the COF crystallites, which is consistent with previous studies using small organic molecules.[38] Nevertheless, the presence of catechol-PNIPAm in contrast to catechol-P*n*BuA indicated a different behavior from the polymer chain, which could be due to polymer/monomer interactions via hydrogen bonding.

Representative SEM micrograph and corresponding elemental mapping with energy dispersive X-ray (EDX) spectroscopy were acquired to confirm the presence of PNIPAm$_{25}$ polymer (**Figure 5**A). Nitrogen and sulfur atoms respectively come from the NIPAm repetitive units and the chain-end derived from the chain-transfer agent (CTA), both elements are distributed throughout the particles, confirming the homogeneous grafting of catechol-PNIPAm$_{25}$ on the COF-5 particles. For COF-catechol-PNIPAm$_{50}$ (Figure S26, Supporting Information) and COF-catechol-PNIPAm$_{100}$ (Figure S27, Supporting Information), only nitrogen atoms were visible due to the $\overline{DP_n}$ increase and consequently the lower sulfur ratio. EDX spectra also confirmed the presence of nitrogen and sulfur atoms by the appearance of the characteristic peaks (N Kα = 0.392 keV and S Kα = 2.307 keV)

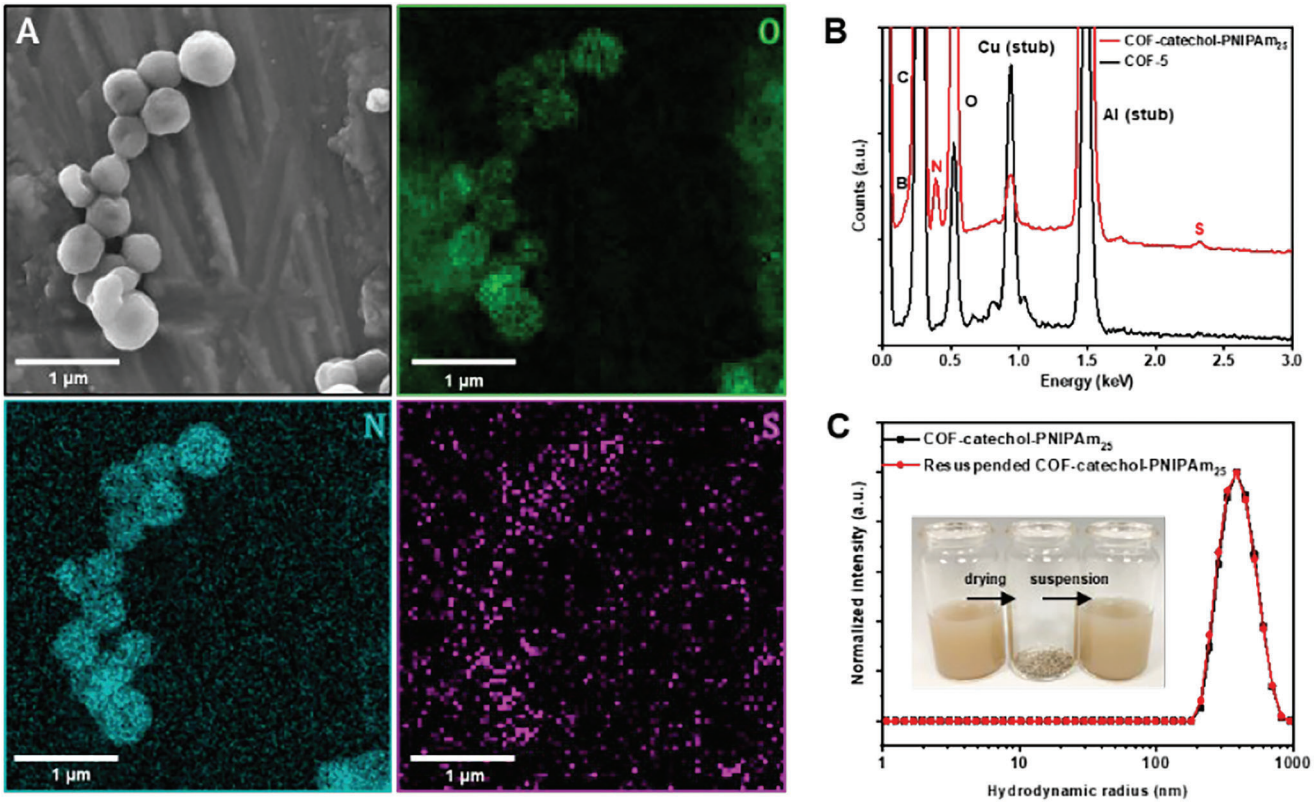

Figure 5. A) Representative SEM micrograph of COF-catechol-PNIPAm$_{25}$ particles and corresponding elemental mapping (O, N, S), B) EDX spectra of COF-5 particles without polymer and COF-catechol-PNIPAm$_{25}$ particles, C) hydrodynamic radius distribution by DLS of COF-catechol-PNIPAm$_{25}$ particles before drying and after resuspension (inset: picture of the suspensions and dried particles).

for all the COF-catechol-PNIPAm samples compared to colloidal COF-5 (Figure 5B and Figure S28, Supporting Information). Interestingly, while isolating COF particles without undesirable co-crystallization remains a challenge in the fields, these spherical COF-catechol-PNIPAm particles can be dried, stored as a powder under argon for several weeks and resuspended in acetonitrile with no change in size as attested by DLS measurements (Figure 5C).

To better understand the mechanism of COF-polymer particle formation depending on the nature of the polymer used, both DLS characterizations (**Figure 6**A) and TEM observations of particles during their formation (Figure 6B,C) were performed. For COF-catechol-P*n*BuA, similarly to the COF-5 particles without polymer, the hydrodynamic radius is constant, about 60 nm, over their formation duration. TEM micrographs of COF-catechol-P*n*BuA after only 30 min of synthesis show anisotropic particles with visible lattice fringes on most of them (Figure 6B). After 2 h of reaction, the single-crystal character of the particles can be clearly attested. TEM micrographs acquired after 6 h show the self-assembly of this sub-units to finally reach their final architecture into quasi-spherical particles (Figure 6B). On the contrary, the R_h of COF-catechol-PNIPAm$_{25}$ increases during their formation, from 200 nm at t_0 to 350 nm after 20 h, and then slightly decreases to reach 300 nm (Figure 6A). TEM micrographs after 30 min reveal amorphous particles, which are gradually enriched with material over time, leading to the formation of larger particles with a jagged surface after 6 h and better-defined, more spherical particles after 20 h. Crystallization is a gradual phenomenon starting after 6 h of synthesis with the appearance of the first and non-oriented lattice fringes. After 20 h, the particles show a radial orientation with defects. Thus, a slow reorganization occurs as the particles form to reach the radial single-crystal grain orientation finally observed (Figure 6C).

To determine the role of catechol-P*n*BuA and catechol-PNIPAm in the formation of COF-polymer particles, we investigated the reaction kinetics. The mixtures of HHTP, PBBA, and catechol-polymer (when added), clouded as particles are formed, so the absorbance measurements at various temperatures provided a means to measure the rate and the activation energies. The absorbance was monitored at 550 nm, at this wavelength, absorbance from traces of oxidized HHTP monomer is negligible (Figure S29, Supporting Information) so the increase in absorbance is due to the turbidity rise. As previously reported for COF-5 powder,[48] COF-5 particle formation started after a short induction period, from 2 min at 80 °C to 8 min at 60 °C (**Figure 7**A and Figure S30A, Supporting Information).

In addition, because the initial rate of COF-5 particle synthesis was temperature-dependent and followed a linear Arrhenius relationship, we calculated the activation energy (E_a) to be 20–22 kcal mol^{-1} (average on three different samples) (Figure S30A, Supporting Information). This value is comparable to the one calculated for COF-5 powder (22–27 kcal mol^{-1}).[48] The addition of 0.045 equiv. of catechol-P*n*BuA/PBBA slightly slowed down the initial rate of particle formation but did not influence the E_a

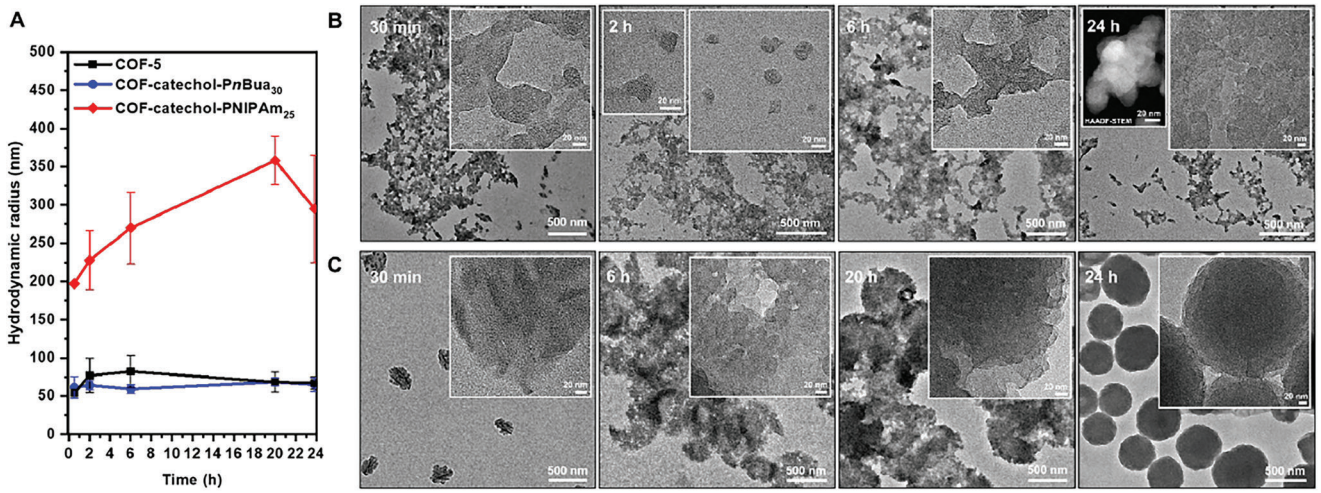

Figure 6. A) Evolution of the hydrodynamic radius obtained by DLS of COF-5 particles without polymer and COF-catechol-polymer particles (average values from three samples and associated standard deviations), B) HRTEM micrographs of COF-catechol-P*n*BuA$_{30}$ particles and C) TEM micrographs of COF-catechol-PNIPAm$_{25}$ particles at different reaction times showing their structural evolution.

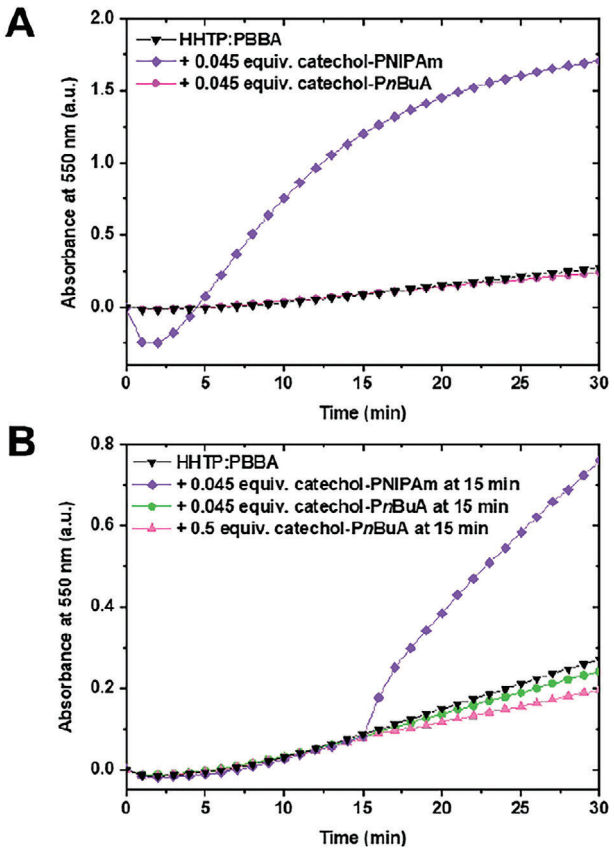

Figure 7. A) Particle formation over time at 70 °C for COF-5 without polymer (HHTP:PBBA) and COF-polymer with 0.045 equiv. of catechol-P*n*BuA or catechol-PNIPAm/PBBA. B) Addition of catechol-polymer at 15 min, showing an increase in absorbance with 0.045 equiv. of catechol-PNIPAm/PBBA and modulating effect with 0.045 and 0.5 equiv. of catechol-P*n*BuA/PBBA.

value calculated (17–22 kcal mol^{-1}) (Figure 7A and Figure S30B, Supporting Information). These observations combined with the absence of catechol-P*n*BuA polymer in the particles indicated that it acted as a modulator of the COF-5 synthesis, thanks to the chain-end catechol moiety acting as a competitor of HHTP. The addition of only 0.045 equiv. of catechol-PNIPAm/PBBA showed a very different effect. As described above, mixing HHTP, PBBA and catechol-PNIPAm at room temperature resulted in a cloudy solution. At higher temperatures, a decrease in absorbance was first observed that replaced the induction period, indicating a reorganization step. Then, the initial rate was clearly accelerated highlighting an enhancement of the particle formation thanks to the catechol-PNIPAm (Figure 7A and Figure S30C, Supporting Information). The initial rate of COF-catechol-PNIPAm formation exhibited a linear temperature dependence but on a larger temperature range from 50 °C, the E_a calculated (19-21 kcal mol^{-1}) was similar to those of COF-5 and COF-catechol-P*n*BuA. To confirm these two phenomena, i.e., modulation by catechol-P*n*BuA and acceleration by catechol-PNIPAm, the two polymers were added after the onset of turbidity (Figure 7B). While the addition of 0.045 equiv. of catechol-PNIPAm/PBBA immediately increased the absorbance and the rate of particle formation, the necessary amount of catechol-P*n*BuA/PBBA to visibly decrease the absorbance was significantly higher. Indeed, for 0.045 equiv. of catechol-P*n*BuA/PBBA added, the ratio of non-productive catechol (from polymer) to productive catechol (from HHTP) moieties is very low and the competitive effect moderate. Consequently, in presence of catechol-PNIPAm, we hypothesized a preorganization via hydrogen bonding between amide groups belonging to the polymer chains and alcohol groups from the monomers and a modulating effect of the catechol-P*n*BuA due to the chain-end functionality. Overall, these results demonstrate that the addition of catechol chain-end functionalized polymer not only acts as a modulator but also can induce a template effect, influencing the size, shape, and crystal grain orientation in the resulting COF-catechol-polymer particles.

3. Conclusion

The development of COF combined with linear polymers is of increasing interest but still in its infancy. We presented here an original example of linear polymers driving the formation of COF particles. The addition of catechol-P*n*BuA resulted in the self-assembly of crystallites into quasi-spherical structures and catechol-PNIPAm led to the preparation of raspberry-like COF-polymer particles. Combination of scanning and transmission electron microscopies (SEM and TEM) and 4D STEM-ACOM highlighted the single-crystal character of the sub-units constituting the COF-catechol-PNIPAm particles and their radial orientation. The presence of PNIPAm chains on the particle surface allowed their drying and storage as powders and their resuspension. Catechol-polymers can be used not only as modulators but also as macromolecular templates introducing supramolecular self-assembly properties into colloidal COF-5 to create new morphologies with higher structural complexity, beyond the framework level. We demonstrated that the addition of judiciously chosen polymers in COFs allowed to create a new landscape of particle morphologies with oriented porosity. The next step will be to capitalize on these results by investigating their emerging properties for various applications. We believe that this simple preparation method, combined with the wide variety of polymers and COFs to be combined, will enable the development of exciting hybrid materials with control over multiscale organization.

4. Experimental Section

Materials: 1,4-Phenylenebis(boronic acid) (PBBA) (96% of purity), 2,3,6,7,10,11-hexahydroxytriphenylene (HHTP) (95% of purity), pinacol, propargyl alcohol, 4-dimethylaminopyridine, *N*-(3-dimethylaminopropyl)-*N*′-ethylcarbodiimide hydrochloride, anhydrous 1,4-dioxane stabilized with BHT, mesitylene (>97% of purity), acetonitrile (HPLC plus gradient), and methanol were purchased from commercial sources and used without further purification. 2,2′-azobis(isobutyronitrile) (AIBN, ≥98%, Aldrich) was recrystallized from methanol, *N*-isopropylacrylamide (NIPAm, ≥98%, Aldrich) was recrystallized from *n*-hexane, *n*-butyl acrylate) (*n*BuA, ≥98%, Aldrich) was purified on silica, acid-CTA (2-(1-isobutyl) sulfanylthiocarbonylsulfanyl-2-methylpropionique acid) and catechol-CTA (*N*-(3,4-dihydroxyphenylethyl)−2-(1-isobutyl) sulfanylthiocarbonylsulfanyl-2-methylpropionamide) were synthesized as previously reported.[49]

Synthesis of Alkyne-CTA: In a round bottom flask, 2-(1-isobutyl) sulfanylthiocarbonylsulfanyl-2-methylpropionique acid (acid-CTA) (4.0 g, 15.87 mmol, 1 eq.), propargyl alcohol (3,14 g, 52,38 mmol, 3.3 eq.), 4-dimethylaminopyridine (3.13 g, 23,81 mmol, 1.5 eq.) and *N*-(3-dimethylaminopropyl)-*N*′-ethylcarbodiimide hydrochloride (4.56 g, 23.81 mmol, 1.5 eq.) were solubilized in 30 mL of dry dichloromethane. The reaction was performed overnight at room temperature, under stirring. The organic phase was washed with acid (HCl) and then basic (NaOH) aqueous solutions, dried with $MgSO_4$, and the solvent was removed under reduced pressure. The residue was purified on a chromatography column (SiO_2, ethyl acetate/petroleum ether: 1/9). alkyne-CTA was obtained as a sticky yellow product with a 71% yield.

RAFT Synthesis of Alkyne-PnBuA: For a degree of polymerization of 25, a solution of alkyne-CTA (90.7 mg, 3.12×10^{-1} mmol), AIBN (10.3 mg, 6.24×10^{-2} mmol), and *n*BuA monomer (1 g, 7.80 mmol) in anhydrous *N,N*-dimethylformamide (2 mL) was prepared. This solution was deoxygenated by bubbling argon for 20 min and then heated to 80 °C under stirring. The solution was cooled down to room temperature and the polymer recovered by precipitation in *n*-hexane. It was purified further by one extra precipitation from acetone into a mixture of water-methanol (1/1 v/v) to obtain a pure product after drying overnight under vacuum.

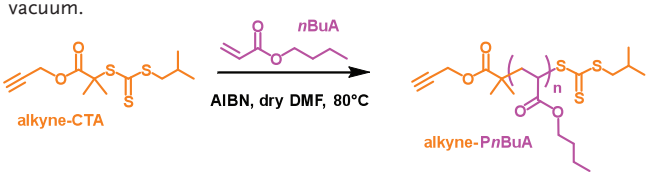

RAFT Synthesis of Catechol-PnBuA: For a degree of polymerization of 25, a solution of catechol-CTA (120.9 mg, 3.12×10-1 mmol), AIBN (10.3 mg, 6.24 × 10-2 mmol), and *n*BuA monomer (1 g, 7.80 mmol) in anhydrous *N,N*-dimethylformamide (2 mL) was prepared. This solution was deoxygenated by bubbling argon for 20 min, then heated to 80 °C under stirring. The solution was cooled down to room temperature and the polymer recovered by precipitation in *n*-hexane. It was purified further by one extra precipitation from acetone into a mixture of water-methanol (1/1 v/v) to obtain a pure product after drying overnight under vacuum.

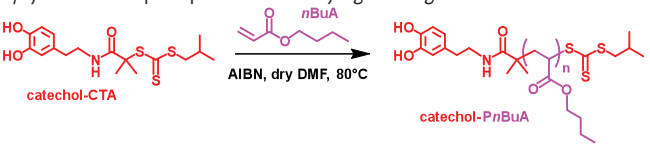

RAFT Synthesis of Catechol-PNIPAm: For a degree of polymerization of 25, a solution of catechol-CTA (137.0 mg, 3.53×10^{-1} mmol), AIBN (11.6 mg, 7.07×10^{-2} mmol), and NIPAm monomer (1 g, 8.84 mmol) in anhydrous *N,N*-dimethylformamide (2 mL) was prepared. This solution was deoxygenated by bubbling argon for 20 min and then heated to 70 °C under stirring. The solution was cooled down to room temperature and the polymer recovered by precipitation in *n*-hexane. It was purified further by one extra precipitation from acetone into *n*-hexane to obtain a pure product after drying overnight under vacuum.

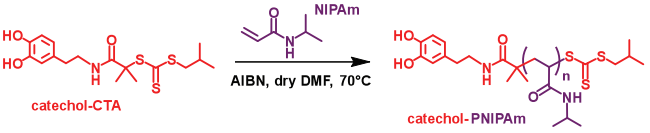

The experimental conditions and the molecular characteristics of the various polymers obtained are summarized in Table S1 (Supporting Information).

Conditions for Synthesis of Colloidal COF-5: In a vial, MeOH (227 µL, 5.62 mmol) was added to 1,4-phenylenebis(boronic acid) (PBBA) (31 mg, 1.87×10^{-1} mmol), and then a dioxane/mesitylene (4:1 v/v, 5 mL) solution was poured. This solution was sonicated for 3 min (37 kHz, 100 W). In another vial, 5 mL of the same solution of dioxane/mesitylene was added to 2,3,6,7,10,11-hexahydroxytriphenylene (HHTP) (40.5 mg, 1.25×10^{-1} mmol) and was sonicated for 3 minutes. This solution was added to the first one with PBBA monomer. This solution was sonicated 3 minutes, then filtered (0.45 µm on PTFE) and mixed with CH_3CN (40 mL). Additional mixture of CH_3CN/dioxane/mesitylene was added to reach a concentration of 1.5 mM in HHTP. The final solution was sonicated for 1 minute, then heated for 24 h to 70°C under atmospheric pressure.

Conditions for Synthesis of Colloidal COF-Polymers: In a vial, MeOH (227 µL, 5.62 mmol) was added to 1,4-phenylenebis(boronic acid) (PBBA) (31 mg, 1.87×10^{-1} mmol), and then a dioxane/mesitylene (4:1 v/v, 5 mL) solution was poured. This solution was sonicated for 3 min (37 kHz, 100 W). In another vial, 5 mL of the same solution of dioxane/mesitylene was added to 2,3,6,7,10,11-hexahydroxytriphenylene (HHTP) (40.5 mg, 1.25×10^{-1} mmol) and was sonicated for 3 min. This solution was added to the first one with PBBA monomer. This solution was sonicated 3 min, then filtered (0.45 µm on PTFE) and mixed with CH_3CN (40 mL). Additional mixture of CH_3CN/dioxane/mesitylene was added to reach a concentration of 1.5 mM in HHTP, this solution was sonicated for 1 min, a solution of alkyne-P*n*BuA, catechol-P*n*BuA or catechol-PNIPAm was added (0.045 eq./PBBA). The vial was manually shaken and heated for 24 h at 70 °C under atmospheric pressure.

Removal of Excess Polymer: To remove the excess polymer in the COF-PNIPAm and COF-PnBuA suspensions, they were centrifuged (12 000 rpm for 10 min) and the supernatant was removed. Acetonitrile was added to the pellet and a vortex was used to suspend the COF-polymer particles, the process was repeated several times until the absence of polymer in the supernatant was verified by ^{1}H NMR.

Proton Nuclear Magnetic Resonance: Proton nuclear magnetic resonance (^{1}H NMR) spectra were recorded on a Bruker 300 MHz FT-NMR spectrometer at room temperature. Deuterated dimethylsulfoxide (DMSO-d_6), deuterated chloroform, or deuterated acetonitrile (acetonitrile-d_3) from Eurisotop was used as the solvent, and chemical shifts (δ) were given in parts per million (ppm).

Compositional Analysis by ^{1}H NMR: The composition of the COF-polymer particles synthesized was determined by ^{1}H NMR. The COF-catechol-PNIPAm and COF-catechol-P*n*BuA suspensions were centrifuged (12 000 rpm for 10 min) and the supernatant was removed. Acetonitrile was added to the pellet and a vortex was used to suspend the COF-polymer particles, the process was repeated several times until the absence of polymer in the supernatant was verified by ^{1}H NMR. The particles were dried under vacuum overnight, and digested by the addition of pinacol in DMSO-d_6 for COF-catechol-PNIPAm and in acetonitrile-d_3 for COF-catechol-P*n*BuA. To quantify the quantity of catechol-PNIPAm we calculated the integration ratio of the six hydroxyl protons on HHTP to the two hydroxyl protons and the three aryl protons of the catechol moiety on the polymer.

Size Exclusion Chromatography (SEC): Size-exclusion chromatograms were recorded using an Alliance system from Waters. Three columns in series from Waters were used: Styragel HR 1 (7.8 × 300 mm), Styragel HR 3 (7.8 × 300 mm), and Styragel HR 4 (7.8 × 300 mm) with THF (+ 0.1% of toluene as flow marker) as eluant with a flow rate of 1 mL min^{-1}. The detector used was a Wyatt Optilab T-Rex differential refractometer detector. The system was thermostated at 35 °C. Polystyrene (PS) standards from 820 to 640,000 g mol^{-1} were used for calibration.

Light Scattering Measurements: Mono-angle dynamic light scattering (DLS) measurements were carried out in 10 mm quartz cells from Hellma with the Malvern Instruments Zetasizer Ultra, which uses a laser source (He-Ne 4 mW) with a wavelength of 633 nm and a scattering angle of 173°. After synthesis, particle size was determined at 25 °C. The autocorrelation functions ($g_1(t)$) were analyzed in terms of relation time distribution (τ) (Equation 1) using the cumulants method.

$$g_1(t) = \int A_{(\tau)} \exp\left(\frac{-t}{\tau}\right) d\tau \quad (1)$$

Hydrodynamic radius (R_h) was determined from the following Stokes-Einstein relation (Equation 2).

$$R_h = \frac{k_B T}{6\pi\eta_s D_0} \quad (2)$$

where D_0 is the diffusion coefficient, η_s is the viscosity of the solvent, T is the absolute temperature in Kelvin, and k_B is the Boltzmann constant.

Ultraviolet–Visible Spectrometry: A Cary 3500 Scan UV–vis spectrometer equipped with a multicell Peltier temperature controller was used. Solutions were placed in 10 mm quartz cells from Hellma. Turbidity was measured by collecting absorbance at 550 nm at various temperatures during COF-5 and COF-polymer formation.

Scanning Electron Microscopy (SEM): This work was carried out on the electron microscopy facility of the advanced characterization platform of the Chevreul Institute. A drop of COF or COF-polymer suspension was deposited on an aluminum stub. In the case of insulating samples (such as COF or polymer) a metallization is necessary. A carbon metallization (thickness of about 200 Å) was carried out using a carbon evaporator (Auto 306 Edwards). The observations were made on a JEOL JSM 7800F LV (Electron Microscopy Platform) equipped with an EDX (Energy Dispersive X-ray Spectroscopy) X-Max SDD detector (Oxford Instruments). Secondary electron images and chemical elemental EDX analyses were acquired with an accelerating voltage of 5 keV and a working distance of 10 mm to limit polymer degradation.

TEM Sample Preparation: Two drops of a COF or COF-polymer suspension were deposited on a carbon film-supported copper grid. The suspension was left on the grid for five seconds and the excess was removed with a filter paper. The grids were then placed in a vacuum desiccator until use.

Transmission Electron Microscopy (TEM): This work was carried out on the electron microscopy facility of the advanced characterization platform of the Chevreul Institute. Transmission electron microscopy (TEM) micrographs were recorded on a Titan Themis at 200 kV with a CCD camera CETA (ThermoFischer) or on a Tecnai G2-20 twin operated at 200 kV with a CCD Gatan Orius camera (low dose).

Automated Crystal Orientation Mapping (ACOM): This work was carried out on the electron microscopy facility of the advanced characterization platform of the Chevreul Institute. ACOM was carried out with the Tecnai in nanobeam diffraction (NBD with a probe between 5 and 10 nm). To avoid damage or superposition, samples were examined with an increment of 10 nm and a dwell time of 10 or 20 ms. The 4D STEM method was applied,[50] from the optical camera filming the fluorescent screen, the diffraction images were acquired in synchronization with the position of the beam on the sample using the Digistar control unit of the Nanomegas system. From a single acquisition of the reciprocal space (4D STEM), it was possible to reconstruct crystalline orientation and virtual Bright and virtual Dark-Field images from separate diffraction events. "Flowline mapping" was used to understand the continuity of a crystal structure by representing each lattice reflection found at a specific scan position (x, y) as a colored and oriented line.[50] The processing was done in Python with the opensource package py4DSTEM.[51]

Wide-Angle X-Ray Scattering (WAXS): Wide-angle X-ray scattering measurements were performed at the Advanced Characterization Platform of the Chevreul Institute and carried out owing to a Xeuss 2.0 apparatus (Xenocs) with a GeniX3D micro-source (λ_{Cu} = 1.54 Å). The suspensions were introduced in capillaries of 1.5 mm outside diameter and 0.01 wall thickness (Hilgenberg), with a silver behenate reference. The sample-to-detector distance was ≈0.35 m and the analysis time was 6 h.

Surface Area and Porosity Measurements: Measurements by N_2 adsorption were performed at 77 K using the Micromeritics Tristar II instrument. Before analysis, a known mass (≈70 mg) of solid was treated at 130 °C under vacuum for 6 h. It is then exposed to ultrapure nitrogen up to 1 atm. The specific surface area (S_{BET}) was calculated using the Brunauer–Emmett–Teller (B.E.T.) method, on the linear part of the B.E.T. plot ($p/p0 = 0.11–0.15$). The pore volume was calculated using the adsorption branch of the isotherms at a $p/p0$ value of 0.99. The pore size distribution was given by the density functional theory (DFT) model. CO_2 adsorption (99.99995, Air Liquide) experiments were carried out on a porosity analyzer (Micromeritics ASAP 2020). A Dewar filled with water and connected to an isothermal bath (Huber Pilot One) was used to keep the temperature at 298 K during the experiment. In the specific case of ultra-microporous solids, the BET surface was measured by single point measurement at $p/p0 = 0.003$.

Supporting Information

Supporting Information is available from the Wiley Online Library or from the author.

Acknowledgements

This work was supported by the Agence Nationale de la Recherche (ANR program COPOCO ANR-21-CE06-0021). The Chevreul Institute was thanked for its help in the development of this work through the ARCHI-CM project supported by the "Ministère de l'Enseignement Supérieur de la Recherche et de l'Innovation", the region "Hauts-de-France", the ERDF program of the European Union and the "Métropole Européenne de Lille". The authors thank Aurélie Malfait and Maxence Épinat for the SEC analyses, Dr David Fournier for providing Alkyne-CTA, Dr Maya Marinova for her

help in carrying out the work on the electron microscopy facility of the Advanced Characterization Platform of the Chevreul Institute and Dr Jérémy Dhainaut from l'Unité de Catalyse et Chimie du Solide (UCCS UMR 8181) for his assistance with gas sorption and BET analyzes. Basile Gautheron, Corinne Henry, and Isabelle Samain are thanked for their help.

Conflict of Interest

The authors declare no conflict of interest.

Data Availability Statement

The data that support the findings of this study are available in the supplementary material of this article.

Keywords

covalent organic frameworks, nanostructured particles, poly(*N*-isopropylacrylamide), polymers, radial single-crystal grain orientation

Received: May 3, 2023
Revised: July 26, 2023
Published online:

[1] A. P. Cote, A. I. Benin, N. W. Ockwig, M. O'Keeffe, A. J. Matzger, O. M. Yaghi, *Science* **2005**, *310*, 1166.
[2] R. P. Bisbey, W. R. Dichtel, *ACS Cent. Sci.* **2017**, *3*, 533.
[3] Y. Zeng, R. Zou, Y. Zhao, *Adv. Mater.* **2016**, *28*, 2855.
[4] Z. Wang, S. Zhang, Y. Chen, Z. Zhang, S. Ma, *Chem. Soc. Rev.* **2020**, *49*, 708.
[5] J. Liu, G. Han, D. Zhao, K. Lu, J. Gao, T.-S. Chung, *Sci. Adv.* **2020**, *6*, eabb1110.
[6] S. Khalil, M. D. Meyer, A. Alazmi, M. H. Samani, P.-C. Huang, M. Barnes, A. B. Marciel, R. Verduzco, *ACS Nano* **2022**, *16*, 20964.
[7] S. Lin, C. S. Diercks, Y.-B. Zhang, N. Kornienko, E. M. Nichols, Y. Zhao, A. R. Paris, D. Kim, P. Yang, O. M. Yaghi, C. J. Chang, *Science* **2015**, *349*, 1208.
[8] Y. Peng, Y. Huang, Y. Zhu, B. Chen, L. Wang, Z. Lai, Z. Zhang, M. Zhao, C. Tan, N. Yang, F. Shao, Y. Han, H. Zhang, *J. Am. Chem. Soc.* **2017**, *139*, 8698.
[9] Z. Meng, K. A. Mirica, *Chem. Soc. Rev.* **2021**, *50*, 13498.
[10] C. R. DeBlase, K. E. Silberstein, T.-T. Truong, H. D. Abruña, W. R. Dichtel, *J. Am. Chem. Soc.* **2013**, *135*, 16821.
[11] A. M. Evans, I. Castano, A. Brumberg, L. R. Parent, A. R. Corcos, R. L. Li, N. C. Flanders, D. J. Gosztola, N. C. Gianneschi, R. D. Schaller, W. R. Dichtel, *J. Am. Chem. Soc.* **2019**, *141*, 19728.
[12] G. Zhang, X. Li, Q. Liao, Y. Liu, K. Xi, W. Huang, X. Jia, *Nat. Commun.* **2018**, *9*, 2785.
[13] T. Huo, Y. Yang, M. Qian, H. Jiang, Y. Du, X. Zhang, Y. Xie, R. Huang, *Biomaterials* **2020**, *260*, 120305.
[14] D. Rodríguez-San-Miguel, F. Zamora, *Chem. Soc. Rev.* **2019**, *48*, 4375.
[15] A. Natraj, W. Ji, J. Xin, I. Castano, D. W. Burke, A. M. Evans, M. J. Strauss, M. Ateia, L. S. Hamachi, N. C. Gianneschi, Z. A. ALOthman, J. Sun, K. Yusuf, W. R. Dichtel, *J. Am. Chem. Soc.* **2022**, *144*, 19813.
[16] P. J. Waller, F. Gándara, O. M. Yaghi, *Acc. Chem. Res.* **2015**, *48*, 3053.
[17] J. Hu, S. K. Gupta, J. Ozdemir, H. Beyzavi, *ACS Appl. Nano Mater.* **2020**, *3*, 6239.
[18] K. Dey, S. Mohata, R. Banerjee, *ACS Nano* **2021**, *15*, 12723.
[19] F. Haase, P. Hirschle, R. Freund, S. Furukawa, Z. Ji, S. Wuttke, *Angew. Chem., Int. Ed.* **2020**, *59*, 22350.
[20] B. J. Smith, L. R. Parent, A. C. Overholts, P. A. Beaucage, R. P. Bisbey, A. D. Chavez, N. Hwang, C. Park, A. M. Evans, N. C. Gianneschi, W. R. Dichtel, *ACS Cent. Sci.* **2017**, *3*, 58.
[21] A. M. Evans, L. R. Parent, N. C. Flanders, R. P. Bisbey, E. Vitaku, M. S. Kirschner, R. D. Schaller, L. X. Chen, N. C. Gianneschi, W. R. Dichtel, *Science* **2018**, *361*, 52.
[22] T. Ma, E. A. Kapustin, S. X. Yin, L. Liang, Z. Zhou, J. Niu, L.-H. Li, Y. Wang, J. Su, J. Li, X. Wang, W. D. Wang, J. Sun, O. M. Yaghi, *Science* **2018**, *361*, 48.
[23] R. L. Li, N. C. Flanders, A. M. Evans, W. Ji, I. Castano, L. X. Chen, N. C. Gianneschi, W. R. Dichtel, *Chem. Sci.* **2019**, *10*, 3796.
[24] H. S. Sasmal, A. Halder, H. Kunjattu, S., K. Dey, A. Nadol, T. G. Ajithkumar, P. Ravindra Bedadur, R. Banerjee, *J. Am. Chem. Soc.* **2019**, *141*, 20371.
[25] J. Tan, S. Namuangruk, W. Kong, N. Kungwan, J. Guo, C. Wang, *Angew. Chem., Int. Ed.* **2016**, *55*, 13979.
[26] S. Kandambeth, V. Venkatesh, D. B. Shinde, S. Kumari, A. Halder, S. Verma, R. Banerjee, *Nat. Commun.* **2015**, *6*, 6786.
[27] J. Hu, J. Zhang, Z. Lin, L. Xie, S. Liao, X. Chen, *Chem. Mater.* **2022**, *34*, 5249.
[28] Y.-Y. Liu, X.-C. Li, S. Wang, T. Cheng, H. Yang, C. Liu, Y. Gong, W.-Y. Lai, W. Huang, *Nat. Commun.* **2020**, *11*, 5561.
[29] X. Shi, Y. Yao, Y. Xu, K. Liu, G. Zhu, L. Chi, G. Lu, *ACS Applied Materials* **2017**, *9*, 7481.
[30] Y. Zhu, Y. Jin, W. Zhang, In *Hybrid Metal-Organic Framework Covalent Organic Framework Polymers*, Vol. *39*, Royal Society of Chemistry, **2021**, p 344.
[31] Z. Xie, B. Wang, Z. Yang, X. Yang, X. Yu, G. Xing, Y. Zhang, L. Chen, *Angew. Chem., Int. Ed.* **2019**, *58*, 15742.
[32] Y. Wang, M. Xie, J. Lan, L. Yuan, J. Yu, J. Li, J. Peng, Z. Chai, J. K. Gibson, M. Zhai, W. Shi, *Chem* **2020**, *6*, 2796.
[33] C. R. Mulzer, L. Shen, R. P. Bisbey, J. R. McKone, N. Zhang, H. D. Abruña, W. R. Dichtel, *ACS Cent. Sci.* **2016**, *2*, 667.
[34] Q. Sun, Y. Tang, B. Aguila, S. Wang, F. S. Xiao, P. K. Thallapally, A. M. Al-Enizi, A. Nafady, S. Ma, *Angew. Chem., Int. Ed.* **2019**, *58*, 8670.
[35] E. Vitaku, C. N. Gannett, K. L. Carpenter, L. Shen, H. D. Abruña, W. R. Dichtel, *J. Am. Chem. Soc.* **2019**, *142*, 16.
[36] Z. Wang, Q. Yu, Y. Huang, H. An, Y. Zhao, Y. Feng, X. Li, X. Shi, J. Liang, F. Pan, P. Cheng, Y. Chen, S. Ma, Z. Zhang, *ACS Cent. Sci.* **2019**, *5*, 1352.
[37] M. Calik, T. Sick, M. Dogru, M. Döblinger, S. Datz, H. Budde, A. Hartschuh, F. Auras, T. Bein, *J. Am. Chem. Soc.* **2016**, *138*, 1234.
[38] I. Castano, A. M. Evans, H. Li, E. Vitaku, M. J. Strauss, J.-L. Brédas, N. C. Gianneschi, W. R. Dichtel, *ACS Cent. Sci.* **2019**, *5*, 1892.
[39] M. Kalaj, K. C. Bentz, S. Ayala Jr, J. M. Palomba, K. S. Barcus, Y. Katayama, S. M. Cohen, *Chem. Rev.* **2020**, *120*, 8267.
[40] M. Pang, A. J. Cairns, Y. Liu, Y. Belmabkhout, H. C. Zeng, M. Eddaoudi, *J. Am. Chem. Soc.* **2012**, *134*, 13176.
[41] M. Fang, D. Cot, C. Montoro, M. Semsarilar, *Polym. Chem.* **2023**, *14*, 662.
[42] K. Barcus, P.-A. Lin, Y. Zhou, G. Arya, S. M. Cohen, *ACS Nano* **2022**, *16*, 18168.
[43] L. Bellamy, R. Pace, *Spectrochimica Acta Part A: Molecular Spectroscopy* **1971**, *27*, 705.
[44] T. M. Garrett, M. E. Cass, K. N. Raymond, *J. Coord. Chem.* **1992**, *25*, 241.
[45] C. Ophus, *Microsc. Microanal.* **2019**, *25*, 563.
[46] K. C. Kim, T.-U. Yoon, Y.-S. Bae, *Microporous Mesoporous Materials* **2016**, *224*, 294.
[47] A. Mukhtar, N. Mellon, S. Saqib, S.-P. Lee, M. A. Bustam, *SN Applied Sciences* **2020**, *2*, 1.

[48] B. J. Smith, W. R. Dichtel, *J. Am. Chem. Soc.* **2014**, *136*, 8783.
[49] C. Zobrist, J. Sobocinski, J. Lyskawa, D. Fournier, V. Miri, M. Traisnel, M. Jimenez, P. Woisel, *Macromolecules* **2011**, *44*, 5883.
[50] O. Panova, C. Ophus, C. J. Takacs, K. C. Bustillo, L. Balhorn, A. Salleo, N. Balsara, A. M. Minor, *Nat. Mater.* **2019**, *18*, 860.
[51] E. F. Rauch, M. Véron, *Eur Phys J Spec Top* **2014**, *66*, 10701.